

Flow behavior in a contra-rotating transonic axial compressor

S. Abbasi¹ and M. Alizadeh²

¹ Faculty of Mechanical, Arak University of Technology, Arak, 3818141167, Iran

Phone: +988633400663;

² Faculty of Mechanical Engineering, Arak University of Technology, Arak, 3818141167, Iran

ABSTRACT – This study investigated a three-dimensional flow analysis on a two-stage contra-rotating axial compressor using the Navier–Stokes, continuity, and energy equations with Ansys CFX commercial software. In order to validate the obtained results, the absolute and relative flow angles curves for each rotor in radial direction were extracted and compared with the other investigation results, indicating good agreement. The compressor efficiency curve also was extracted by varying the compressor pressure ratio and compressor efficiency against mass flow rate. The flow results revealed that further distortion of the flow structure in the second rotor imposed a greater increase in the amount of entropy, especially at near-stall conditions. The increase of entropy in the second rotor is due to the interference of the tip leakage flow with the main flow which consequently caused more drops in the second rotor, suggesting that more efficacy of flow control methods occurred in the second rotor than in the first rotor.

ARTICLE HISTORY

Received: 04th Jan 2021

Revised: 28th Mar 2021

Accepted: 05th June 2021

KEYWORDS

*Axial compressor;
contra-rotating;
numerical simulation;
performance curve.*

INTRODUCTION

A compressor of a conventional gas turbine engine is made of rotating rotors mounted on a shaft and rotated at the same direction. But contra-rotation is a concept which rotors rotate alternately in opposite directions. Contra-rotation or rotation of rotors in opposite directions is one of the efficient methods that significantly improves the aerodynamic performance of compressors, turbines, and fans. Stator blades can be removed from the compressor using contra-rotating technology. As a result, the weight of the engine is also reduced and the thrust-to-weight ratio is significantly increased. Moreover, the momentum caused by the movement of the aircraft due to the rotation of the engine shaft is reduced by applying contra-rotating on the blades. This improves the performance and stability of the aircraft greatly. There has been a considerable emphasis upon the research on the contra-rotating turbomachines. In recent years, institutes all over the world have committed themselves to develop high-performance engines. As an example, F-119 and Trent-900 engines are produced by the PW company and the Rolls–Royce Company, respectively. Both of these engines are of the contra-rotating turbine type which have good performance. Many researchers have studied on the field of contra-rotating turbines [1-3]. Some of the initial attempts at contra-rotation were informed in the early 1940s [4]. Their studies showed that applying compressor stages with adjacent contra-rotation improves the flow structure and the engine efficiency as well. An increase in the pressure ratio and flow capacity in this turbomachine has also been reported. Smith [5] and Zak [6] have experimentally investigated the multi-stage contra-rotating compressor. Their findings indicated that by decreasing the axial spacing between the blade rows, an increase in efficiency and static pressure coefficient was achieved. Liu et al. [7] results consistent with those of Smith [5] and Zak [6], investigated the effect of the axial spacing of the blade rows on the contra-rotating compressor.

Lynam et al. [8] investigated the performance of contra-rotating axial fans and reported a significant performance improvement. Young [9] investigated contra-rotation axial flow fans at an equal rotational speed. His results showed that the use of contra-rotating rotors at design condition leads to increase the pressure ratio and mass flow rate. In their research, off-design conditions have not been studied and evaluated though. Sharma et al. [10, 11] evaluated the performance by varying the axial spacing between the rotors. Their findings indicated that the large axial spacing causes the maximum pressure ratio to occur at a lower mass flow rate. Besides, the smaller spacing between rotors reduces the formation of stall cells at the first rotor. Wang et al. [12] experimentally and numerically investigated the effect of tip clearance size on the performance of the contra-rotating compressor. They confirmed that by increasing the tip clearance size, the stall margin, and the isentropic efficiency decreased and the flow unsteadiness increased. It was also found that increasing the tip clearance size had more negative effects on the performance of the upstream rotor.

Unsteady flows in the mixing area between the rotors. Strong unsteady interactions between the rotors may lead to large acoustic noise emission [13] and may affect the performances of the stage [14, 15]. Shigemitsu et al. [16] compare two counter-rotating pumps with the same front rotor and two different rear rotors. They conclude that the pressure field of the front rotor is strongly influenced by the rear rotor. The unsteady pressure fluctuations are dominated by the rear rotor blade passing frequency, and are located close to the front rotor. In subsequent works [17, 18], they also compare a counter-rotating pump with a rotor-stator stage and perform Laser Doppler Velocimetry measurement, focusing on the rotor-rotor interaction at partial flow rate. They propose that decreasing the rear rotor rotational speed and stagger angle

would be beneficial for the stable operation of the pump, by suppressing the back flow region at the inlet tip region of the rear rotor. They eventually observe that the blockage effect of the rear rotor on the flow field close to the front rotor blades trailing edges seems stronger than the effects of the front rotor wake on the rear rotor. The effect of the axial distance between the counter-rotating rotors of an axial-flow fan is studied by Shigemitsu et al. [19]. They conclude that the influence of this distance on static pressure rise is stronger at partial flow rate than at design flow rate. The axial distance exhibits a slight influence on the static pressure rise of the front rotor, the static pressure of the rear rotor decreasing gradually as the distance increases above 1:25 mean chord length of the front rotor blades.

The use of compressors with contra-rotating rotors reduces the weight and length of the motor and improves its performance. However, it is necessary to identify the efficiency and details of flow structures of contra-rotating compressors at different engine operating conditions. It highlights the complexities of using this method and its contribution for improving performance strategies. A review of research literature shows that although many studies have been carried out on the use of these types of compressors and turbines in low speed and the performance of high speed compressors and their complex flow structures at different operating conditions have not yet been identified. In this study flow analysis of a two-stage contra-rotating compressor with rotor-stator-rotor configuration is investigated and its overall performance is extracted. It also examined the details of the flow structure at different engine operating conditions, the flow behavior in different components of the compressor is extracted and compared. Investigation of the boundary layer, shock wave, and tip leakage flow interaction at different operating conditions and their influence on flow field characteristics such as pressure, Mach number, and entropy leads to a deeper understanding of the various phenomena in the transonic axial compressor.

COMPRESSOR GEOMETRY AND MESHING

In the present study, a two-stage contra-rotating axial compressor with rotor-stator-rotor configuration is considered. The geometry of the compressor is extracted from reference [13]. Table 1 lists some characteristics of this axial compressor.

Table 1. Characteristic of the contra-rotating axial compressor [13]

Parameter	First rotor	First stator	Second rotor
Inlet Radius (Hub) (mm)	212.5	218.7	225.8
Exit Radius (Hub) (mm)	216.7	224.7	229
Inlet Radius (Tip) (mm)	287.3	282.2	274.1
Exit Radius (Tip) (mm)	284	275.3	271.3
Number of blades	28	36	38
Axial Speed (RPM)	18000	-----	-18000

A multi-block structured grid system has been employed using Ansys TurboGrid. The surface mesh structure is shown in Figure 1. The computational field for a passage is involved to be 393664 for the first rotor, 454770 for the second rotor, and 204102 for the stator. The whole grid system consisted of about 1052536 cells for the whole compressor. Mesh structure should be of sufficient density especially in the blade tip clearance region and near solid walls to be able to resolve the flow characteristics precisely. The mesh density near the solid walls ensured y^+ values to be kept at less than 5, which enabled the viscous sub-layer to be resolved, precisely. In this meshing, the tip size is considered to be 1% of the blade span.

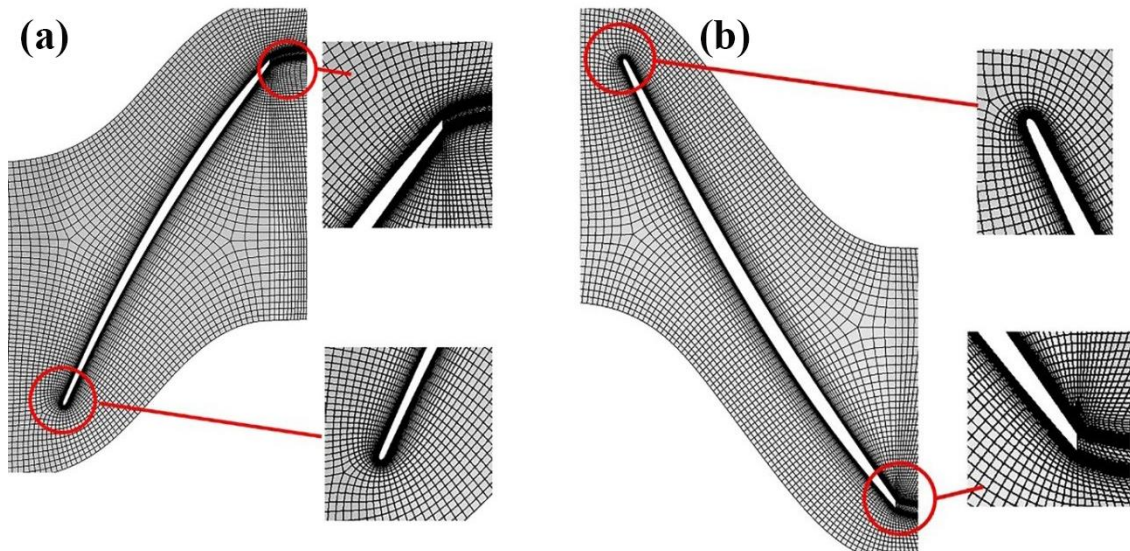


Figure 1. Rotor blade mesh (a) first rotor (b) second rotor

In order to ensure the meshing and the number of computational networks, in the present simulation, the independence of the results from the number of grid has been investigated. For this purpose, current meshing has been done in six different types and the performance of the compressor in each of them has been investigated. In Table 1 the values of pressure and efficiency ratios in different numbers of element are illustrated.

It is known that as the number of element from 500000 computing cell to 1052536 computing cell increases, the values of pressure ratio and efficiency change. However, by increasing the number of elements from 1052536 the computing cell to 1300000 computing cell, there is no significant change in the performance characteristics of the compressor. Therefore, the 1052536 number of elements is appropriate for the present analysis and this networking has been used.

Table 2. The values of pressure and efficiency ratios in different numbers of element

Number of Element	Pressure Ratio	Efficiency
500000	2.4059	81.0011
700000	2.422	81.3774
950000	2.432	82.4741
1052536	2.4326	83.5774
1200000	2.4326	83.674
1300000	2.4326	83.674

BOUNDARY CONDITION AND SETUP

The solver selected in this study is Ansys-CFX commercial software capable of simulating 3D and viscous flows. The software uses the finite volume method to solve the governing equations including momentum, continuity, and energy. Turbulent flows in turbomachines are three-dimensional and viscous. These features are due to the complex structure of the limiting walls and the presence of boundary layers, tip and secondary leakage currents, rotational effects, pressure gradients and the geometric shape of the blades and their torsion. On the other hand, tip leakage current has a great effect on the performance and stability of axial compressors. The $k-\omega$ -SST turbulence model was employed to derive Reynolds stresses. It is an efficient method that has shown good results in predicting the flow behaviour performance of various turbomachines.

Multiple reference frames were used in this study. As a result, it was possible to divide the compressor into the stationary and rotating parts, concerning an inertial frame. A frozen rotor interface was used between two domains. The rotation axis of the first rotor and the second rotor are set in the opposite direction. Figure 2 shows the geometry and boundary conditions. The total pressure (339 kPa) and total temperature (488 K) are set at the inlet boundary while static pressure is applied at the outlet boundary. To analyze different operating conditions, the static pressure at the compressor outlet has been changed. Since only one passage of compressors was considered, the periodic boundary conditions were imposed for the repeating boundaries. No-slip and adiabatic wall conditions were imposed all over the solid walls.

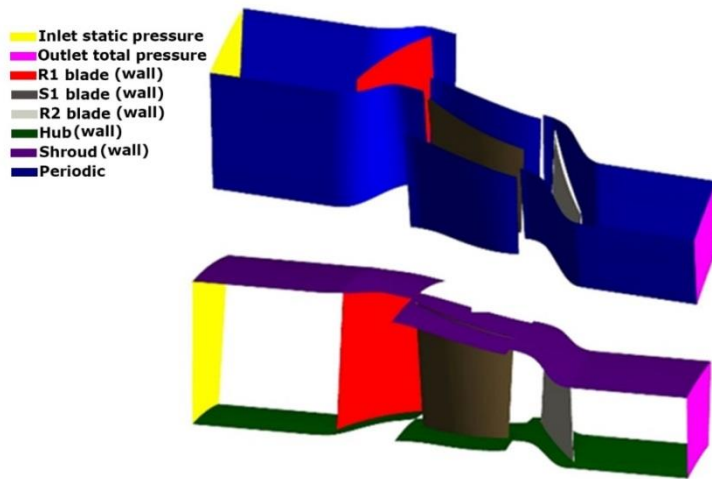


Figure 2. Boundary conditions

VALIDATION

To validate the results, the changes of absolute and relative flow angles at different radial distances are compared with the reference results [13] in Figures 3 and 4 which is shown the accuracy of the numerical results.

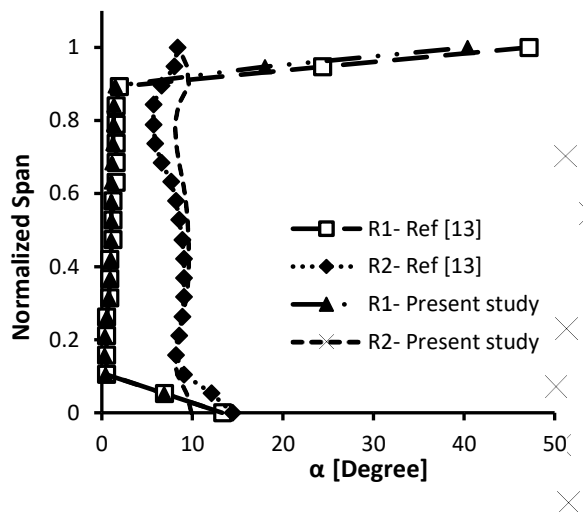


Figure 3. The comparison of numerical and reference study [13] absolute flow angles curves at first and second rotors

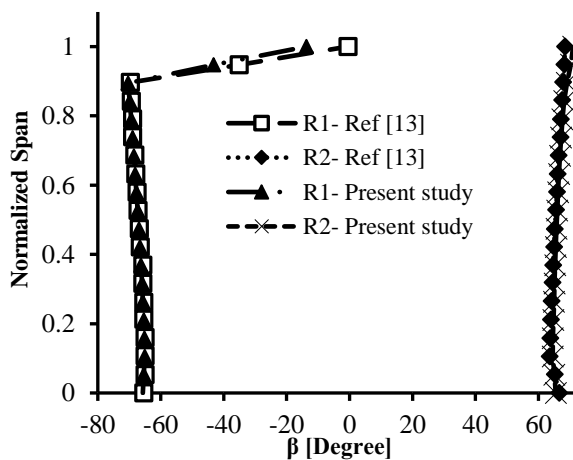


Figure 4. The comparison of numerical and reference study [13] relative flow angles curves at first and second rotors

RESULTS

The compressor map curve including total pressure ratio and efficiency against mass flow rate has been derived. Figures 5 and 6 illustrate these curves. It is evident that, like conventional compressors, the pressure ratio increases with decreasing mass flow rate.

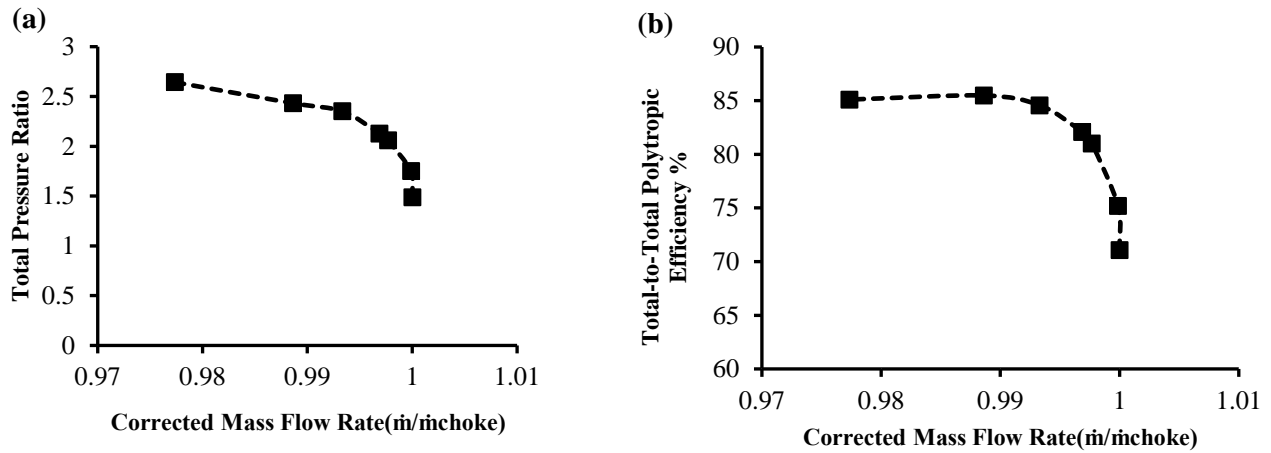


Figure 5. Compressor performance map: (a) Total pressure ratio and (b) polytropic efficiency vs. corrected mass flow rate

To the deeper understanding of the details of the flow structure in the contra-rotating compressor, the results have been extracted at various operation conditions including choke, design, and near-stall conditions. Figure 6 shows the relative total pressure of the flow at 0.97 spans. Streamlines have also been added to this contour. The occurrence of the vertical flows at near-stall conditions is obvious. This leads to blocking the flow moving through the blade passage. Besides, there are no reverse and vortex flows at design and choke conditions. One of the important results that can be obtained from this contour is recognizing the interface of the main flow and the tip leakage flow. This interface is shown by black lines in Figure 6. It is clear that by reducing the mass flow rate from choking to near-stall condition, the interface line moves from the blade trailing edge to the leading edge and even upstream. This feature is due to a decrease in main flow strength and an increase in tip leakage flow at the near stall condition.

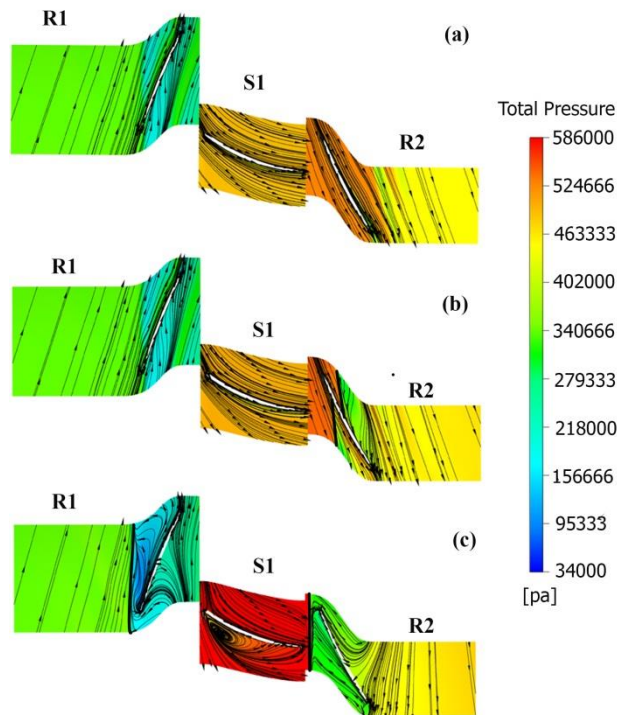


Figure 6. Distribution of total pressure at 0.97 span plane with relative velocity streamlines at three mass flow rates: (a) choke point (b) design point and (c) near-stall point

Figure 7 shows the relative Mach contour at 0.97 spans at different operating conditions. Due to a decrease in mass flow rate from choke to near-stall conditions, the relative Mach number has been decreased. In these contours, sudden changes in Mach number and shock waves are observed. At the choking mass flow rate (Part A in Figure 7), shock waves are visible near the trailing edge of the rotor. As the mass flow rate decreases toward the design conditions (Figure 7 b, c), the shock waves move upstream from the trailing edge and approach the leading edge. Generating a shock wave results in a pressure loss in the flow field and an increase in entropy.

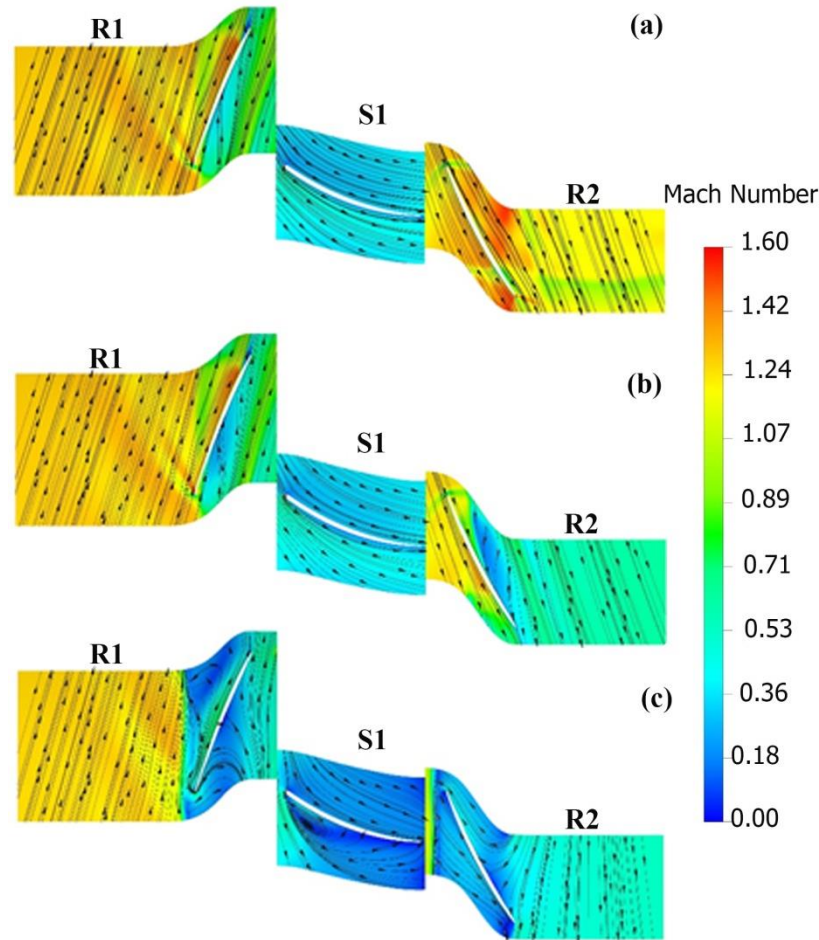


Figure 7. Contours of relative Mach number at 0.97 span plane with relative velocity streamlines at three mass flow rates: (a) choke point, (b) design point and (c) near-stall point

Figure 8 shows the distribution of pressure loading at 0.97 span plane at different operating conditions. This figure is important because the pressure difference on the airfoil surface (i.e., pressure and suction) in the rotors is the reason for the tip leakage flow. In this figure, the upper curve at each mass flow rate corresponds to the pressure side and the lower curve to the suction side. It is evident that with decreasing mass flow rate, from choke to near-stall conditions, the pressure difference between the two sides increases. This results in increased tip leakage flow, resulting in stronger vortices in the rotors and more blockage in the flow passage.

In the choke and design conditions, the sudden increase in pressure at the beginning of the first and second rotor blades is due to the occurrence of shock waves. However, under near-stall conditions, due to a decrease in mass flow rate and consequently a decrease in relative velocity, no strong shock waves have occurred. Therefore, the static pressure at the beginning of the rotor did not increase significantly.

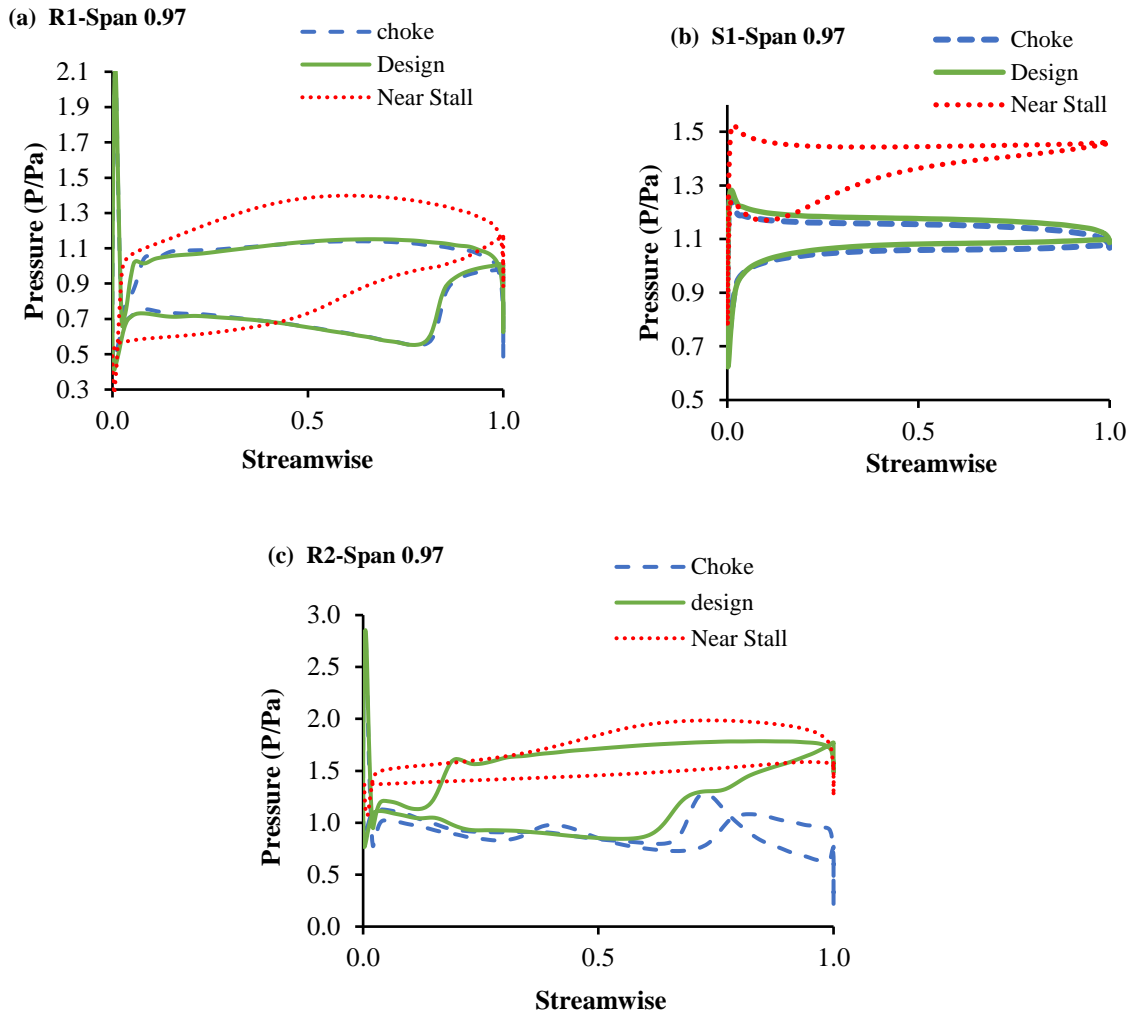


Figure 8. Pressure load curves on the pressure and suction sides of the compressor at different operating conditions of the compressor (at 0.97 span): (a) first Rotor (b) first Stator (c) second Rotor

Figure 9 shows the entropy coefficient vs the streamwise direction through the compressor at different operating conditions. As illustrated in Figure 9, the position of the first rotor blade is between 0.6 to 0.94 and the second rotor is between 2 and 2.4. It is clear that in all operating conditions, the entropy coefficient of the flow before the first rotor is equal. But as the flow enters the rotor, the entropy increases at once. This is due to the occurrence of shock waves as shown in Figure 7. After leaving flow from the rotor, the associated losses such as profile loss, tip leakage flow loss, and so on are disappeared. This results in a decrease in the whole losses in the flow structure and consequently a decrease in entropy as illustrated in Figure 9.

It is clear that a sudden increase in entropy occurs similarly at all operating conditions. However, due to the occurrence of a stronger tip leakage flow near the stall and the resulting loss, this entropy increase occurs earlier and more than other mass flow rate (i.e., choking and design) to illustrate how the stall cells occur and propagate in the circumferential and radial direction, the axial velocity contour at streamwise direction is shown in Figure 10. One can understand that in near-stall conditions, tip leakage vortex and axial velocity deficient have occurred in areas near the leading edge of the first rotor and stator. The occurrence of these vertices near the tip of the blade is due to the interfere of the tip leakage flow with the main flow. However, in design and choke conditions, such vortexes are not found in any region. The backflows near the tip region of the second rotor are significantly larger than similar flows in other compressor components. It is observed that the counter-rotation of the rotors causes the streamlines in the second rotor (R2) and the stator (S1) to be opposite the direction of the first rotor (R1). As seen in Figure 9, the entropy at the second rotor inlet is increased more than the other parts. Therefore, according to Figures 7, 9, and 10, it is concluded that the occurrence of stronger vortexes at the second rotor inlet and a higher flow velocity, the entropy in this region.

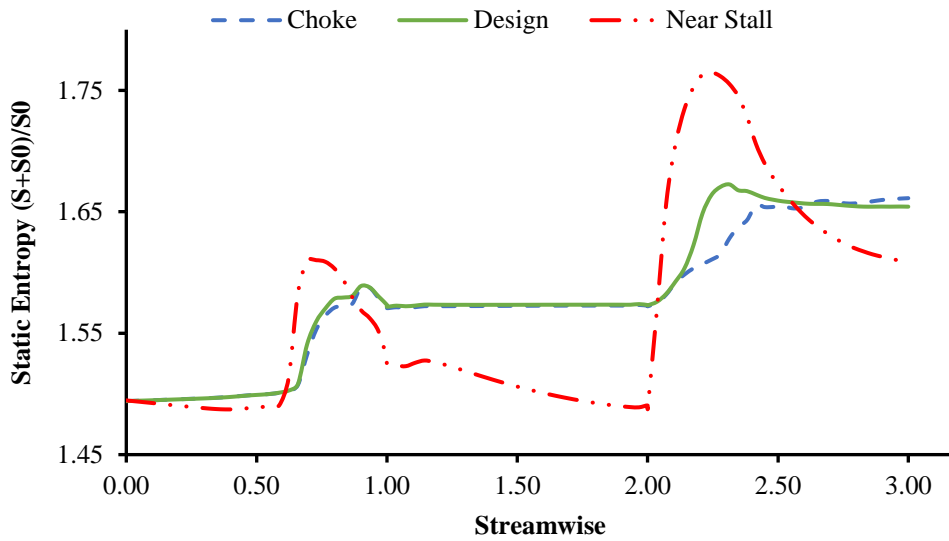
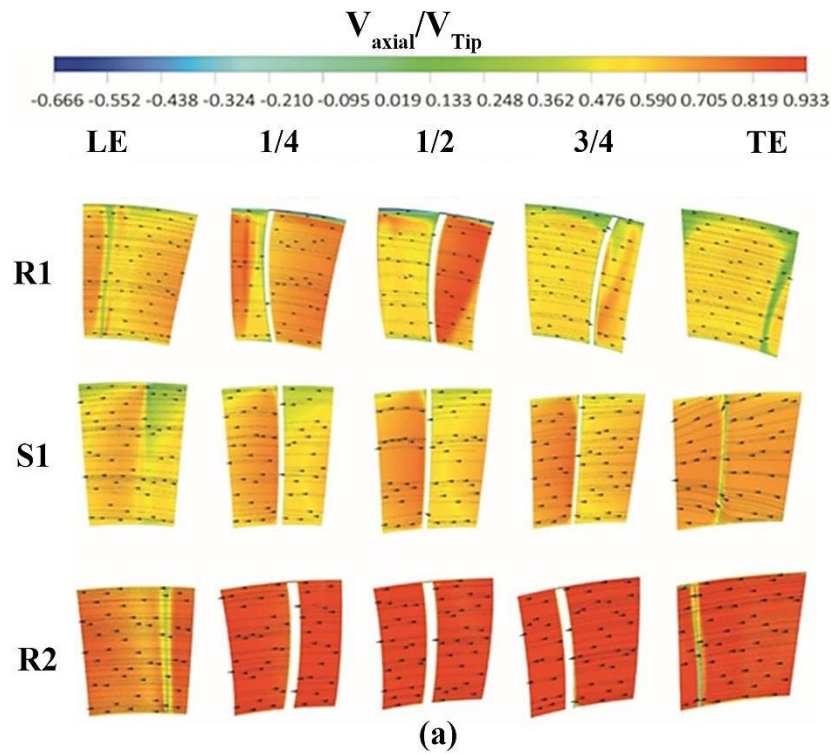


Figure 9. Entropy curves vs streamwise at different operating conditions

As shown in Figure 9, it is evident that with moving in the axial direction from 2 to 2.28 streamwise, the entropy coefficient increases from 1.49 to 1.79. However, this increase in entropy does not exist in the first rotor. The stall cell created near the tip region in stall condition is also clearly visible in Figure 10-c. Moreover, in the first rotor, the stall cells are observed at such positions. In the stator, stall cells occurred at 1/4, 2/4, and 3/4 blade chord and the trailing edge (TE). It is important to study and compare the flow behavior in the first and second rotors. It was found that in the choking and design conditions, flow behavior at the first and second rotors was not significantly different. But in near-stall conditions, the flow structure in the second rotor becomes more disrupted, and consequently stronger stall cells are formed. Accordingly, the entropy produced in the second rotor is much greater than the entropy of the first rotor. It is owing to the stronger shock waves and their interaction with the tip leakage flow in the second rotor.

Consequently, to improve the performance of the compressor in near-stall conditions, it is essential to control the flow structure initially in the second rotor which has a greater effect on the flow behavior of the whole compressor.



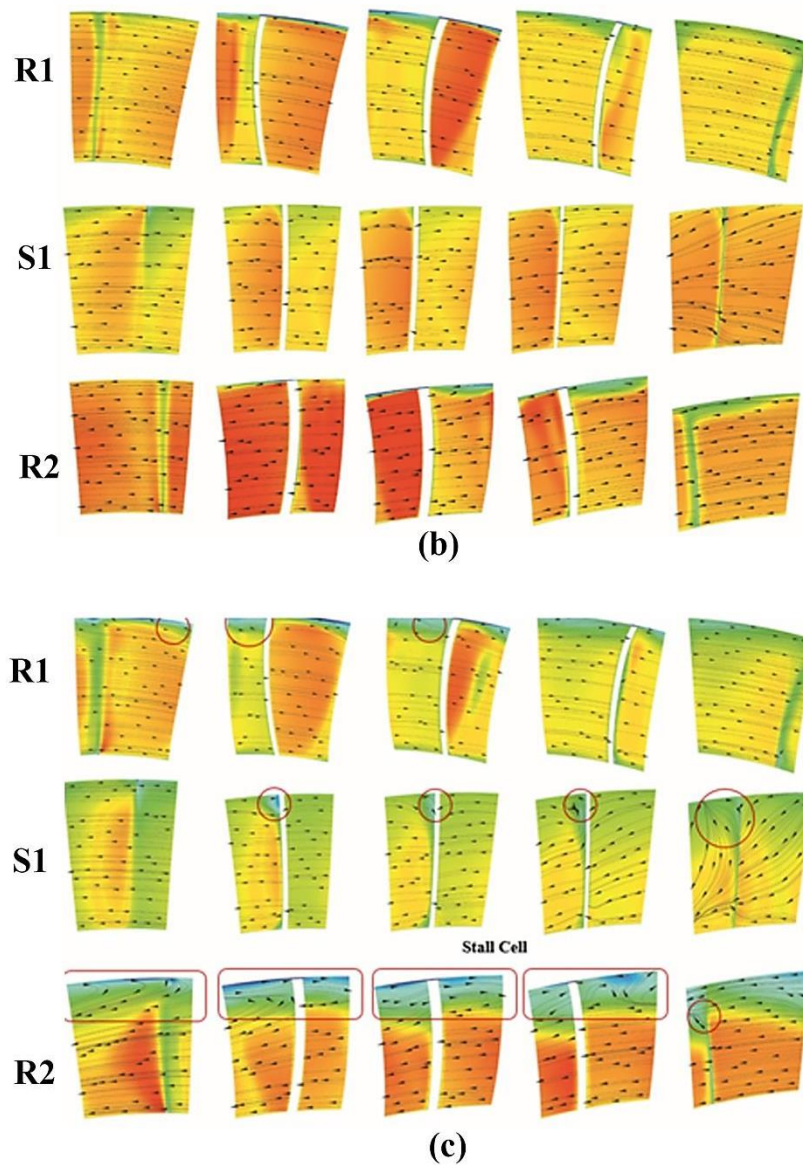


Figure 10. Contours of relative axial velocity to blade tip velocity ratio from different axial portions at different operating conditions: (a) chock, (b) design and (c) near-stall

CONCLUSION

In the present paper, we investigate the performance of a two-stage counter-rotating compressor with rotor-stator-rotor configuration. This combination reduces the weight and length of the compressor by removing the second stator. Three-dimensional flow analysis was performed using Ansys CFX commercial software. Validation of the results was accomplished by comparing the changes of absolute and relative flow angles in the spanwise direction which showed good agreement. The compressor performance map was obtained in terms of the pressure ratio and efficiency vs mass flow rate. To study the flow structure under different operating conditions, the results of the analysis were obtained at three mass flow rates.

It was clear that a sudden increase in entropy occurs similarly in all operating conditions. However, due to the occurrence of a stronger tip leakage flow near the stall and the resulting loss, this entropy increase occurs earlier and more than other mass flow rate (i.e., choking and design). It was found that in the choking and design conditions, flow behavior at the first and second rotors was not significantly different. But in the near-stall conditions, the flow structure in the second rotor becomes more disrupted, and consequently stronger stall cells are formed. Accordingly, the entropy produced in the second rotor is much greater than the entropy of the first rotor. It is owing to the stronger shock waves and their interaction with the tip leakage flow in the second rotor. Consequently, to improve the performance of the compressor in near-stall conditions, it is essential to control the flow structure initially in the second rotor which has more effect on the flow behavior of the whole compressor.

REFERENCES

- [1] H. Wang, Q. Zhao, X. Zhao, and J. Xu, "Unsteady numerical simulation of shock systems in vaneless counter-rotating turbine," in *Turbo Expo: Power for Land, Sea, and Air*, 2005, pp. 477-485.
- [2] L. Ji, J. Chen, H. Huang, and J. Xu, "The key techniques in utilizing vaneless counter-rotating turbine," *Journal of Engineering Thermophysics*, vol. 24, no. 1, pp. 35-38, 2003.
- [3] L. Ji, J. Chen, H. Huang, and J. Xu, "Investigation about effects of axial gap on the performance of vaneless counter-rotating turbine," *Journal of Engineering Thermophysics*, vol. 23, no. 5, pp. 565-568, 2002.
- [4] P. Sharma and A. Adekoya, "A review of recent research on contra-rotating axial flow compressor stage," in *Turbo Expo: Power for Land, Sea, and Air*, June 10-13, 1996, Birmingham, UK.
- [5] L. H. Smith, "Casing boundary layers in multistage axial compressors," *Flow Research on Blading*, pp. 275-304, 1970.
- [6] A. Mikolajczak, "The practical importance of unsteady flow, in unsteady phenomena in turbomachinery," *AGARD paper CP-144*, NATO, 1977.
- [7] X. Mao and B. Liu, "A numerical study on the unsteady effect of axial spacing on the performance in a contra-rotating axial compressor," *Proceedings of the Institution of Mechanical Engineers, Part C: Journal of Mechanical Engineering Science*, vol. 231, no. 14, pp. 2598-2609, 2017.
- [8] F. Lynam and S. Hawes, "Contra rotating axial flow fans," *The engineers*, pp. 1-8, 1946.
- [9] R. Young, "Contra-rotating axial fans," *J. Inst. Heat. Vent. Eng.*, vol. 18, p. 187, 1951.
- [10] P. Sharma, Y. Jain, and D. Pundhir, "A study of some factors affecting the performance of a contra-rotating axial compressor stage," *Proceedings of the Institution of Mechanical Engineers, Part A: Power and Process Engineering*, vol. 202, pp. 15-21, 1988.
- [11] P. Sharma, D. Pundhir, and K. Chaudhry, "A study of some factors affecting the aeroacoustic performance of a ducted contra-rotating axial flow fan stage," in *11th Aeroacoustics Conference*, 1987, p. 2730.
- [12] Y. Wang, W. Chen, C. Wu, and S. Ren, "Effects of tip clearance size on the performance and tip leakage vortex in dual-rows counter-rotating compressor," *Proceedings of the Institution of Mechanical Engineers, Part G: Journal of Aerospace Engineering*, vol. 229, pp. 1953-1965, 2015.
- [13] J. Hurault, S. Kouidri, and F. Bakir, "Experimental investigations on the wall pressure measurement on the blade of axial flow fans," *Experimental Thermal and Fluid Science*, vol. 40, pp. 29-37, 2012.
- [14] J. M. F. Oro, K. M. A. Díaz, C. S. Morros, and E. B. Marigorta, "On the structure of turbulence in a low-speed axial fan with inlet guide vanes," *Experimental Thermal and Fluid Science*, vol. 32, pp. 316-331, 2007.
- [15] J. M. Fernández Oro, K. M. Argüelles Díaz, M. Rodríguez Lastra, M. Galdo Vega, and B. Pereiras García, "Converged statistics for time-resolved measurements in low-speed axial fans using high-frequency response probes," *Experimental Thermal and Fluid Science*, vol. 54, pp. 71-84, 2014.
- [16] T. Shigemitsu, T. Takano, A. Furukawa, K. Okuma, and S. Watanabe, "Pressure measurement on casing wall and blade rows interaction of contra-rotating axial flow pump," *Journal of Thermal Science*, vol. 14, pp. 142-149, 2005.
- [17] T. Shigemitsu, A. Furukawa, S. Watanabe, K. Okuma, and J. Fukutomi, "Experimental analysis of internal flow of contra-rotating axial flow pump," in *Proceedings of the 8th International Symposium on Experimental and Computational Aerothermodynamics of Internal Flows*, Lyon, 2007.
- [18] T. Shigemitsu, A. Furukawa, S. Watanabe, K. Okuma, and J. Fukutomi, "Internal Flow Measurement with LDV at Design Point of Contra-Rotating Axial Flow Pump," *Journal of Fluid Science and Technology*, vol. 4, pp. 723-734, 2009.
- [19] T. Shigemitsu, J. Fukutomi, and H. Shimizu, "Influence of blade row distance on performance and flow condition of contra-rotating small-sized axial fan," *International Journal of Fluid Machinery and Systems*, vol. 5, pp. 161-167, 2012.